aerospace

MDPI

Article

On the Study of Performance Enhancement of 3D Printing and Industrial Application on Aviation Devices

Hui-Pei Chang [1] and Yung-Lan Yeh [2,*]

[1] Department of Occupational Safety and Health, Chang Jung Christian University, Tainan 71101, Taiwan
[2] Master Program in Industrial and Smart Technology, National Chung-Hsing University, Nantou 540, Taiwan
* Correspondence: ylyeh1229@gmail.com; Tel.: +886-0953-287-989

Abstract

Three-dimensional printing is the most commonly used method for producing customized or mock-up products for industrial applications. In particular, aviation devices for drones usually require a high spatial resolution to satisfy the small size requirement. In practical applications of drones, the two main tasks are inspection and detection. However, the working environment is often filled with flammable gases, such as natural gas or petroleum gas. Thus, the parts of drones that can easily produce an electrical spark, such as electronic connectors, should be specially protected. In this study, atmosphere control was applied to enhance the printing performance and manufacture of anti-explosion devices. The results demonstrate that atmosphere control can efficiently improve the print quality and that the print resolution of a commercial 3D printer can be enhanced to reach the mm scale. In the anti-pressure testing via a high-pressure smoke experiment, the manufactured anti-explosion devices for drones showed an appropriate intrinsic safety level, suggesting that they can be used in drones used for daily inspections of pipelines in petrochemical plants. The two main contributions of this study are the development of a practical method for improving FDM 3D printers and an anti-explosion device for drones.

Keywords: 3D printing; drone; atmosphere control; anti-explosion

1. Introduction

Three-dimensional printing technology, also called additive manufacturing, has been developed for decades [1,2]. It is a manufacturing process that continuously adds print material in an additive process, which is controlled by a computer after modeling. Compared to traditional manufacturing, 3D printing technology efficiently minimizes material waste because it primarily uses the layer-by-layer additive production method [3,4]. It is believed that 3D printing will become the main manufacturing method in the future. The related industrial technologies are continuously being improved, and many innovative applications have been developed. In the future, it will have considerable impacts on business, education, the medical field, and people's lives. In particular, 3D technology will likely continue to play a unique role in manufacturing customized products in the foreseeable future.

The advantages of 3D printing include its fast printing speed, use of cheap materials, suitability for use in industrial design, and ability to produce colored objects and scientific and architectural models [5–7]. However, there are also several disadvantages: it has poor resolution, the products are fragile and must be filled with a filler to enhance their strength, and the printing process is easily affected by the surroundings [8,9]. Most consumer 3D

Check for updates

Academic Editor: Pericles Panagiotou

Received: 14 December 2025
Revised: 9 January 2026
Accepted: 11 January 2026
Published: 14 January 2026

Copyright: © 2026 by the authors. Licensee MDPI, Basel, Switzerland. This article is an open access article distributed under the terms and conditions of the Creative Commons Attribution (CC BY) license.

printers are of the FDM type due to their convenience and practicality. FDM printers use many types of materials, including carbon fiber, ABS, PLA, etc., depending on the application. Industrially, 3D printing technology is used in the aerospace [10], building and construction [11], and weapon industries [12]. Three-dimensional printing technology has effectively decreased the number of manufactured parts needed, allows for product customization, and can be used in applications with limited manufacturing space.

In 3D printing, the layer-by-layer additive process prints the product based on a computer 3D model. The melting of the material may occur early or late due to dramatic variations in the environmental temperature, resulting in a final product that does not have the original design shape and does not meet the accuracy requirements. Therefore, atmosphere control in the printing chamber that minimizes external disturbances can enhance the printing quality to produce a final product that matches the original design. Here, the so-called chamber refers to the area that encloses the entire printed area to form a closed region. Initially, atmosphere control was mainly used in the thermal analysis of special manufacturing processes [13–15]. Typically, an inert gas, such as nitrogen or helium, is injected into the printing chamber and forms an internally stable gas recycling system to prevent external influence on the printing process and remove unwanted impurities. Several studies showed that controlling the atmospheric pressure and internal flow rate can improve printing quality [16–18]. The most commonly used methods were thermal or temperature control in a closed space [19–21].

In order to further confirm the improvements in 3D printing accuracy using atmosphere control, this study developed 3D-printed anti-explosion devices for multi-rotor UAVs carrying out inspection tasks in a petrochemical plant area. The most important requirement of anti-explosion devices is accuracy in order to prevent gas leakage. Therefore, these devices require high printing quality and accuracy. All the device designs were modeled using a computer to view all the design details and allow for modifications in the future. The device was manufactured using light-weight, high-density PLA. Because there are no regulations for anti-explosion devices for UAVs, the regulations for industrial anti-explosion devices and grades were used and are provided in Appendix A. It clearly defines the design and manufacture of anti-explosion devices. The design procedure and testing, which conform to the regulations given in Appendix A, will be discussed in the next section. The applicability and installation of the product and the final testing are described in the last section.

Using atmosphere control in the printing chamber to enhance the accuracy and quality of the FDM 3D printing process was the initial focus of this study because of the high precision requirements for anti-explosion devices. A full-scale wind tunnel and a recycling airflow system were constructed to simulate the printing process. Three different kinds of nozzles with different inclined angles were designed based on previous real operational results, with the aim of increasing the efficiency and printing quality without introducing substantial structural changes to the chamber. In addition, the velocity was optimized to enhance the precision and obtain the appropriate control variables. The results of the present work can be used to improve the internal environment of the printing chamber in 3D printing applications and achieve the printing quality needed for anti-explosion devices. This method for the manufacture of a device for UAVs used in petrochemical plants can be used as a platform for verifying other research results.

2. Background and Experimental Setup

The background and experimental setup are described in this section, including the design, printer, wind tunnel system, and measurement systems. All the details on the system's stability are also described.

2.1. UAV

UAVs can be equipped with instruments for industrial plant inspection. However, in this operational environment, there are hazards such as the presence of electricity, pipelines, or flammable gases. Typically, the electrical joints of UAVs are exposed and unprotected. Thus, a spark and explosion due to collision or other hazards could occur during industrial inspection. Consequently, this study developed an anti-explosion shell to cover these electrical joints to prevent them from contacting flammable gases.

Since the UAV will be carrying inspection instruments, the weight should be considered during the design process. Therefore, the special cover for electrical line joints was designed to only insulate the electrical joints instead of covering the entire airframe.

2.2. FDM 3D Printer

The FDM 3D printer used in this paper was self-designed and handmade. It mainly referenced a commercial model for its setup, which made it easy to install the necessary experimental equipment and reduced its cost. To meet the MESG (Maximum Experimental Safe Gap) requirement, a high-precision screw and step motor were adopted for the 3D printer, and its spatial resolution was set to ± 0.05 mm. The customized 3D printer used in this study is shown in Figure 1. It is composed of three traveling mechanisms driven by a servomotor. To enhance the printing quality, the FDM 3D printer was placed inside a metal box to maintain a constant environmental temperature and achieve atmosphere control via introducing air or inert gas.

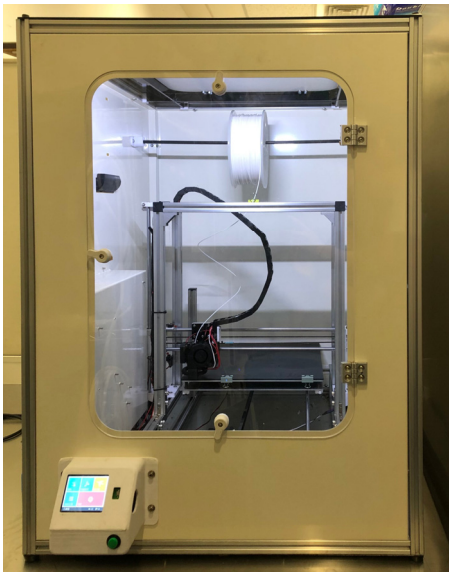


Figure 1. Customized FDM 3D printer with atmosphere control. Spatial resolution was set to ± 0.05 mm.

To simply and shorten the R&D process in this study, PLA, a light-weight material, and a customized FDM 3D printer were used in the preliminary manufacture of an anti-explosion device. In order to conform to the industrial regulations, the designed device was tested using a high-pressure smoke method [22] to determine if there are gaps or gas leakage. In this study, the layer infill was set to 60–80% to enhance the structural density.

2.3. Wind Tunnel

The structure of the wind tunnel imitated the chamber of an actual 3D printer; it was made of acrylic, and all the connection parts were made using PLA via FDM 3D printing. The detailed design of the wind tunnel is shown in Figure 2. The rectangular hole on the

right-hand side of the figure is the location of the inlet nozzle, and the small square hole on the left-hand side is the location of the outlet nozzle. In addition, there is a small round hole for installing the measurement instruments. All the subsystems were designed using SolidWorks 2023 software and made using PLA and FDM 3D printing. The expanded nozzle and compressor adapter were installed as shown in Figure 3 (red frames), which shows the overall architecture.

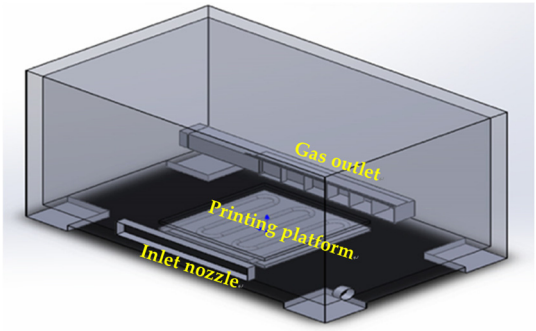


Figure 2. Experimental wind tunnel arrangement with atmosphere control of 3D printer.

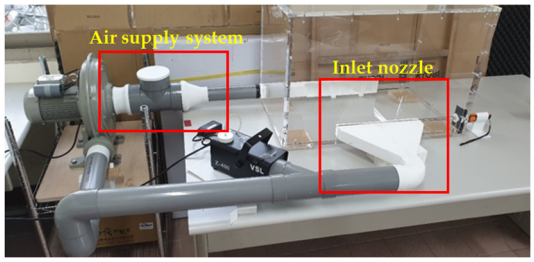


Figure 3. Experimental setup of the wind tunnel.

The grid-shaped outlet is shown in Figure 4a. It has a grid structure and is not expected to perform well because the outlet flow is not concentrated. This outlet is the primary reference benchmark for different experiments. In this study, three additional types of nozzles were designed and used to study the outlet flow concentration, as shown in Figure 4b–d. In addition to different exit numbers and tilde angles, the height and width of these nozzle exits were the same, which were 12 mm and 200 mm, respectively.

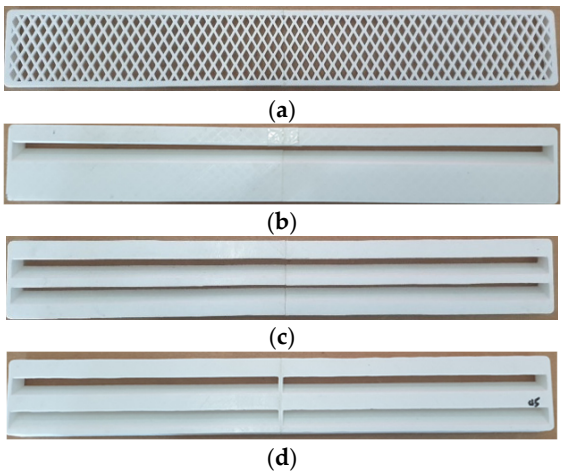


Figure 4. Different nozzle configurations: (**a**) grid-shaped outlet; (**b**) the single-outlet nozzle (downward tilde angle = 30°); (**c**) compound nozzle (downward tilde angle = 30°); (**d**) compound nozzle (upper downward tilde angle = 30° and lower downward tilde angle 45°).

2.4. Measurement Systems

A constant-temperature hot-wire anemometer was used to measure the velocity at the exit of the nozzle. The measurement range was 0 to 30 m/s, and its accuracy was 0.1 m/s ± 5% in the range of 0 to 2 m/s and 0.3 m/s ± 5% when the wind speed was higher than 2 m/s. The velocity spatial resolution was 0.01 m/sec. In order to filter out signal noise and allow for statistical analysis, the measurement time (sampling period) at each point was 15 s, and the sampling rate was fixed at 350 Hz. The shape of the nozzle was symmetrical, so the measurement points were mainly distributed in one half of the nozzle (see Figure 5). All the different nozzles shown in Figure 4 had the same measurement points, respectively.

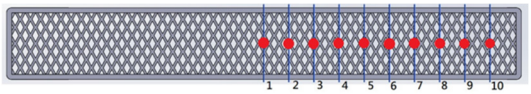


Figure 5. Arrangement of measurement points.

To investigate nozzle performance, a multi-channel thermal measurement system based on a thermal sensor was developed to measure the temperature variation due to wind velocity near the nozzle exit. The initial temperature was set at 40 °C. A faster decline indicates that the influence of wind speed is more significant and vice versa. The resolution of this instrument was about 0.1 °C. To determine the effect of distance, the measurement points were distributed along the centerline from upstream to downstream.

The long-time averaged method was used for the velocity measurements. The sampling rate of the AD converter was fixed at 350 Hz because the velocity in the tunnel was low. The measurement time of each point was 15 s to allow for statistical analysis, which can average out signal noise and provide a consistent flow field. The standard deviation was calculated to further confirm the data concentration and perform error analysis.

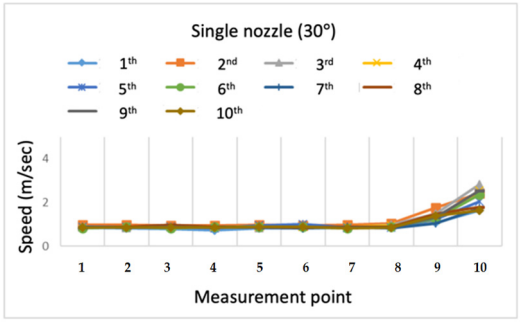
3. Results and Discussion

This section describes and discusses the experimental results. First, airflow calibration was carried out to correct the velocity of the wind tunnel. Temperature measurements were performed to analyze the effects of atmosphere control. Error analysis was applied to enhance the confidence of the measurements. To determine the actual effect, the print quality was confirmed by FDM 3D printing PLA. Next, the design and manufacture of anti-explosion devices was carried out under atmosphere control. The applicability of the designed devices and their adherence to anti-explosion regulations were verified.

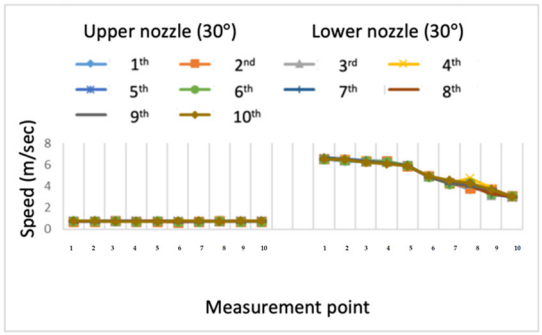
3.1. Atmosphere Control

3.1.1. Airflow Calibration

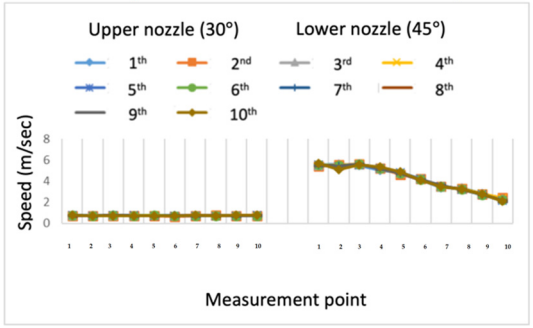
The initial velocities of the different types of nozzles were measured to determine the airflow distributions at the nozzle outlet and apply modifications to achieve a stable flow. As shown in Figure 6a, the velocity distribution of a single 30° tilde nozzle was not well distributed near the right-hand edge. The same phenomenon was seen in other nozzles, including the grid-shaped outlet (Figure 6b,d), indicating that the air supply system was not stable and the air concentration inside the pipeline was not well distributed. Therefore, a tapered deflector was installed inside the expansion section to more evenly distribute the internal airflow (Figure 7). After this modification, the exit velocity distributions of the nozzles considerably improved (Figure 8a,b). This step is important for enhancing the atmosphere control in the chamber because it improves the uniformity of airflow blowing across the product surface, which is the key factor for solidification timing of the material during printing.



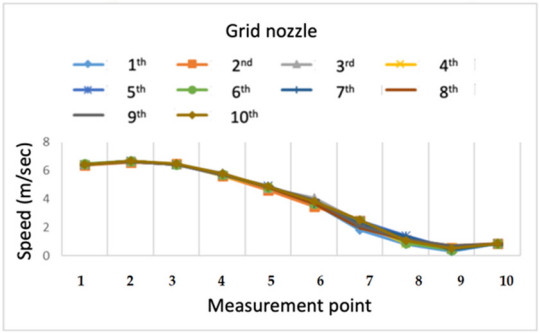
(**a**) Single-outlet nozzle (downward tilde angle = 30°)



(**b**) Compound nozzle of same tilde angles



(**c**) Compound nozzle of different tilde angles



(**d**) Grid-shaped outlet

Figure 6. Velocity distributions at the outlet of the different nozzles without modification.

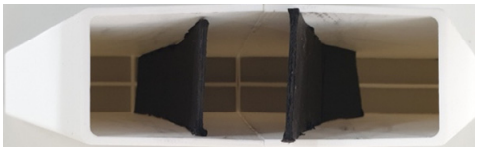
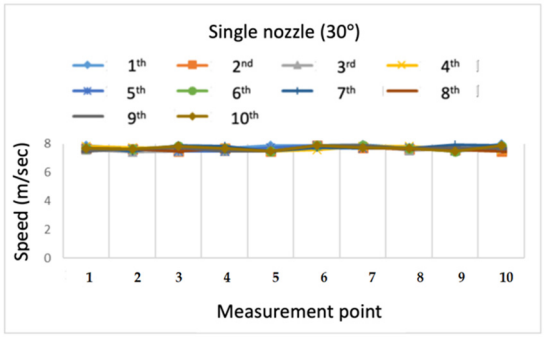
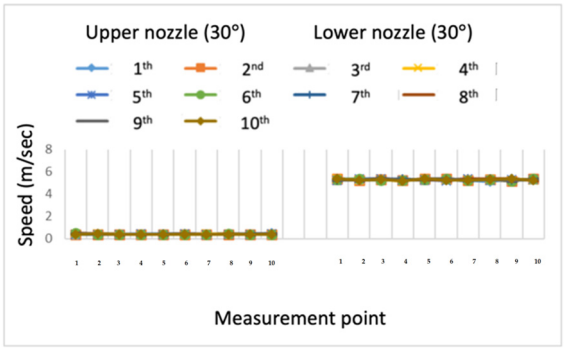


Figure 7. Tapered deflector installed inside the expansion section.



(**a**) Single-outlet nozzle (downward tilde angle = 30°)



(**b**) Compound nozzle of the same tilde angles

Figure 8. Velocity distributions at the outlet of the different nozzles with modification.

However, the experimental results of the dual-output nozzles also revealed that the velocities of the upper and lower output nozzles were not consistent (Figure 8). There are two possible causes for these results. The first one is that the airflow is not uniform when it enters the nozzle, leading to the upper nozzle velocity being greater than the lower nozzle velocity. The second possible cause is due to the location of the hot-wire probe and the nozzle position inside the chamber. The nozzle inside the chamber is in a lower position, which might restrict the space for velocity measurements. However, interestingly, the results of the velocity measurements are in agreement with the requirements. The primary design goal for the dual-output nozzles with different tilde angles was to simultaneously affect the proximal and distal positions of the printing area. The higher the output velocity of the upper nozzle, the stronger the influence of atmosphere control on the airflow at the distal position. Meanwhile, the influence of a lower velocity could satisfy the requirements at the proximal position.

3.1.2. Temperature Measurement

Temperature measurements were also performed to further understand the efficiency of the different types of nozzles. If the nozzle's efficacy is better, the temperature at that position should be lower. As shown in Figure 9, the temperature measurement platform was constructed using six linearly arranged thermal sensors; their initial temperature was set to 40 degrees, which is higher than the environmental temperature. The experimental configuration is shown in Figure 10. The average temperature was mainly used for representation.

In order to enhance the control performance, a holder was installed with the nozzle. The preliminary measurement results without the holder showed that atmosphere control had no obvious effect on the temperature (Figure 11a–c). By contrast, the temperature decrease was more distinct when the holder was installed (Figure 12a–c). All the different types of nozzles showed an average temperature decrement of over two degrees, indicating that the delivery of gas via these nozzles and the holder enhances the atmosphere control.

Furthermore, the results also indicate that the temperature variation was smooth and that the influence of temperature was slightly dependent on the distance from the nozzle. The quality of FDM 3D-printed products could be consistently maintained using this control method.

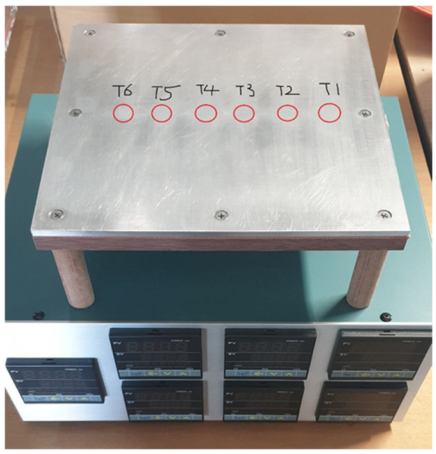


Figure 9. Temperature measurement platform.

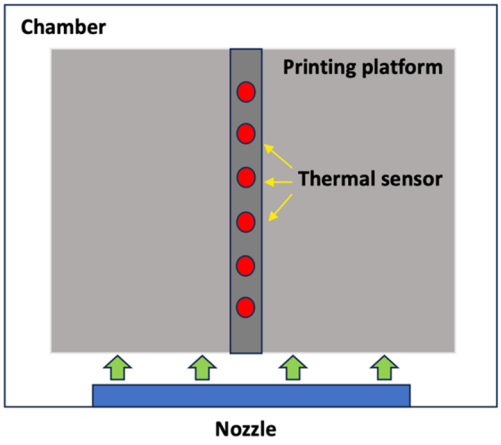
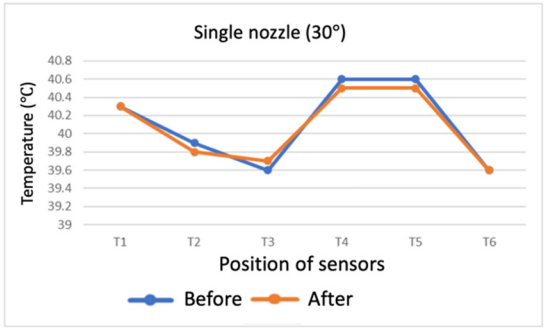
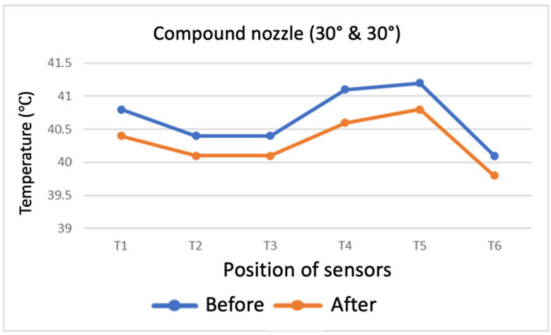


Figure 10. Experimental configuration of the thermal sensor.

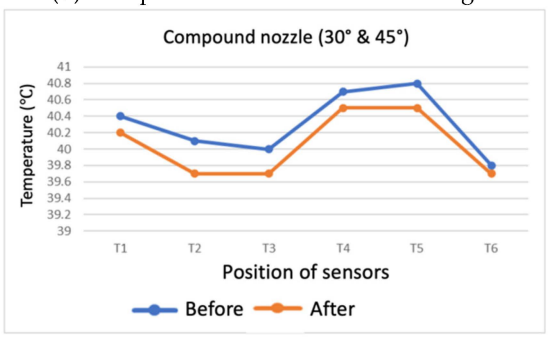


(**a**) Single-outlet nozzle (downward tilde angle = 30°)

Figure 11. *Cont.*

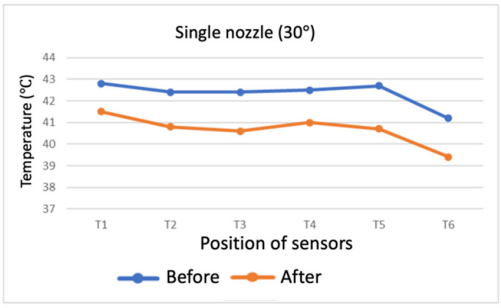


(**b**) Compound nozzle of same tilde angles

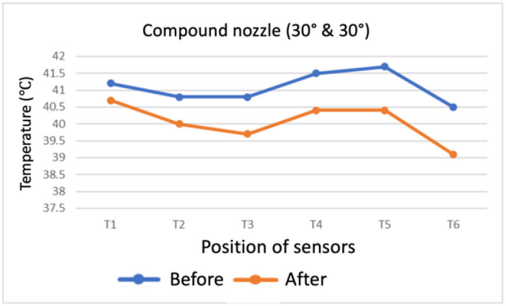


(**c**) Compound nozzle of different tilde angles

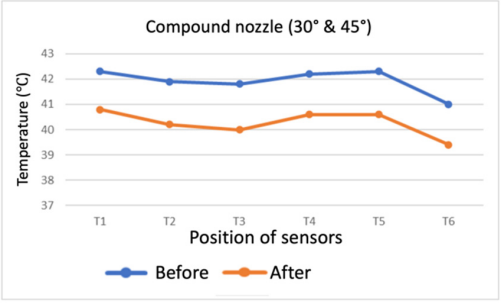
Figure 11. Temperature distributions of different nozzles without modification.



(**a**) Single-outlet nozzle (downward tilde angle = 30°)



(**b**) Compound nozzle of same tilde angles



(**c**) Compound nozzle of different tilde angles

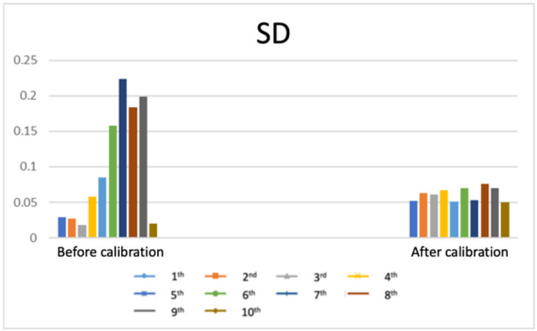
Figure 12. Temperature distributions of different nozzles with modification.

The results reveal a method for improving atmosphere control under vendor-constrained conditions with no adverse effects from the additional structure in the chamber. Most importantly, the cost of this modification is low, and it is easy to implement. This is one of the primary contributions of this research.

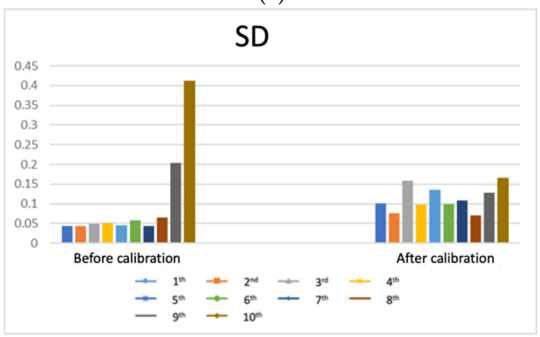
3.1.3. Error Analysis

Error analysis was performed to confirm the accuracy of the experimental data, and the standard deviation (SD) was calculated to measure the data centralization. This is the most commonly used method to reveal the deviation from the mean value. Based on the basic theorem of standard deviation, a smaller value indicates that the experimental data are more concentrated and consistent, and the accuracy and reliability of the experimental data are high.

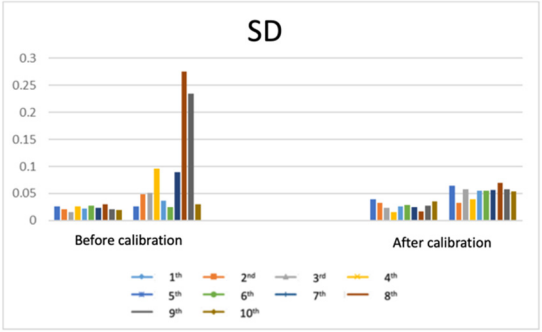
As shown in Figure 13, the variation in SD values before the airflow adjustment showed a nonuniform distribution with values typically lower than 0.4. The airflow adjustment device inside the nozzle resulted in a much more stable airflow at the nozzle outlet, and the unstable variation in airflow also decreased. Consequently, the airflow was much more stable and uniform after airflow calibration, and the distributions of the SD values exhibited more consistency (Figure 13). Furthermore, these values were less than 0.05 and showed smoother distributions than those without the adjustment.



(**a**)

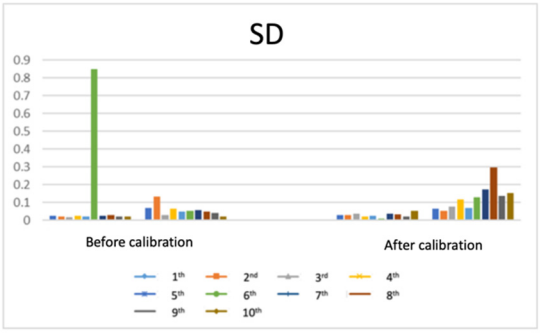


(**b**)



(**c**)

Figure 13. *Cont.*



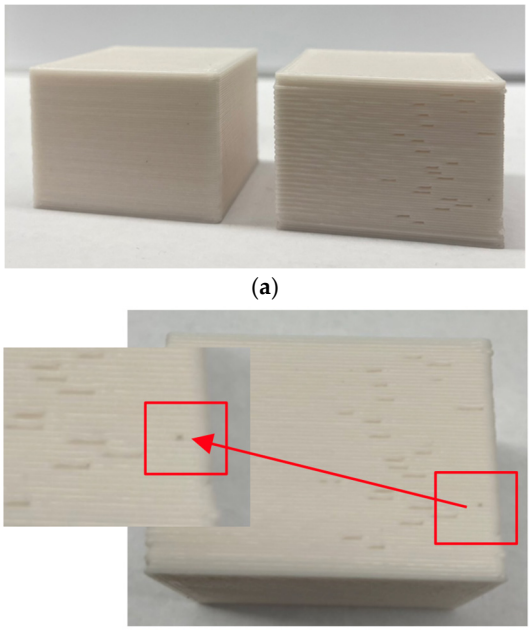
(**d**)

Figure 13. SD distributions of different nozzles with/without modification: (**a**) grid-shaped outlet (average exit velocity = 6 m/s); (**b**) single-outlet nozzle (downward tilde angle = 30°) (average exit velocity = 8 m/s); (**c**) compound nozzle of same tilde angles (average exit velocity = 6 m/s); (**d**) compound nozzle of different tilde angles (average exit velocity = 6 m/s).

3.2. FDM Print Quality Under Atmosphere Control

In the initial design of the wind tunnel, the bottom plate was designed to be disassembled to allow a small-sized printer to be installed. A 3D printer was placed inside the chamber of the wind tunnel, and PLA was used as the main printing material to confirm the efficacy of atmosphere control.

In these comparison experiments, a standard test plate was printed with and without the atmosphere control technology developed in this study. Under the original environmental conditions, the printed plate surface appeared more uniform compared to the plate printed with atmosphere control (Figure 14a). There was also no obvious uneven surface structure due to a nonuniform decrease in the curing temperature. However, the printing quality under atmosphere control using the original grid nozzle was poor, and there was dust on the surface in the case without atmosphere control (Figure 14b), which was caused by the nonuniform temperature decrease.



(**a**)

(**b**)

Figure 14. Comparison of printing quality with/without atmosphere control: (**a**) comparison of products printed without and with atmosphere control; (**b**) dust on the surface.

The effective atmosphere control affects the curing time during printing and strengthens the foundation, which is stacked layer by layer. In addition, the quality of the product, including surface smoothness and strength, is improved. An experiment was carried out to measure the warping of the product. As shown in Figure 15, the warping became worse under higher environmental temperatures. In this experimental setup, the environmental temperature is affected by the sprinkler and heated plate at the bottom, which might result in improper curing timing and stop the printing process because of structural damage (Figure 15b). For this research, such results were sufficient for the experiment requirements. Therefore, other parameters, such as surface roughness and layer shift, etc., were not considered.

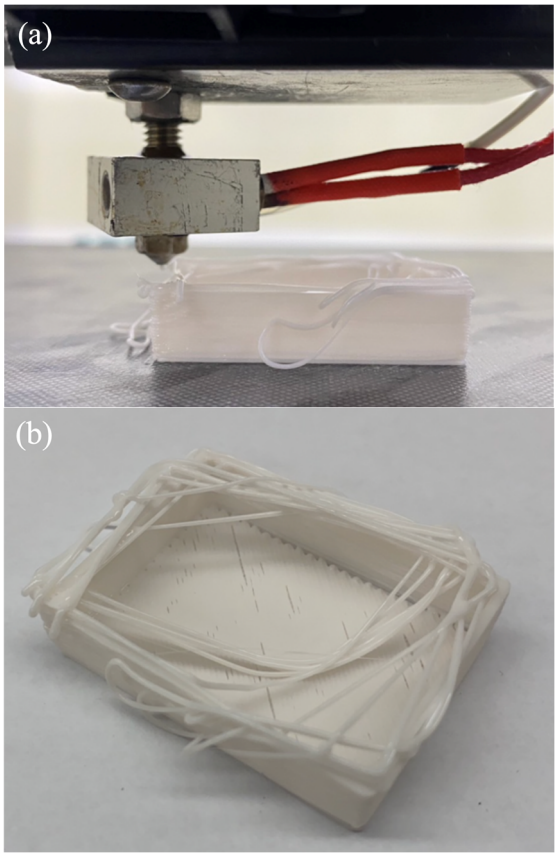


Figure 15. Warping due to temperature effects: (**a**) termination of the printing process; (**b**) structural damage in the printed product.

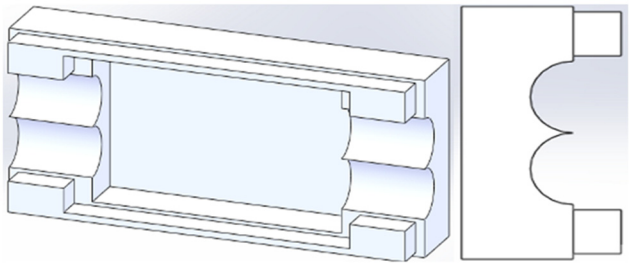
3.3. Construction of Anti-Explosion Device

3.3.1. Design

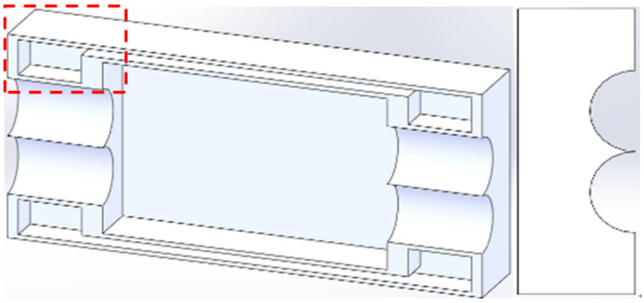
The computer design of the device was based on detailed measurements of electronic connectors (Figure 16a). Its size is about 50 mm long and 30 mm wide. The general space margin used in industrial design was not considered in the first-generation design. Based on this first-generation design, the details of the subsequent designs were modified to optimize the actual assembly. The wiring of UAVs must be considered because of the installation requirements under different wiring conditions. According to the additional space requirement, there should be a large enough space margin for the anti-explosion shell to be accommodated.



(**a**) Electronic connector of a UAV



(**b**) Upper cover

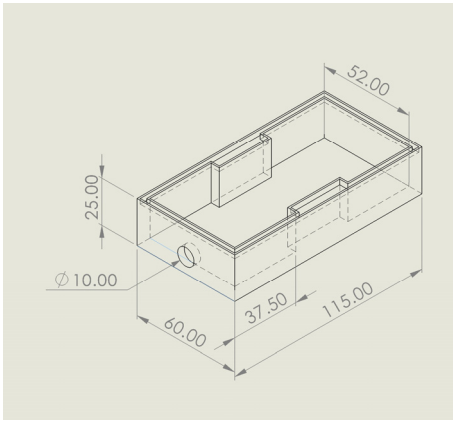


(**c**) Lower cover

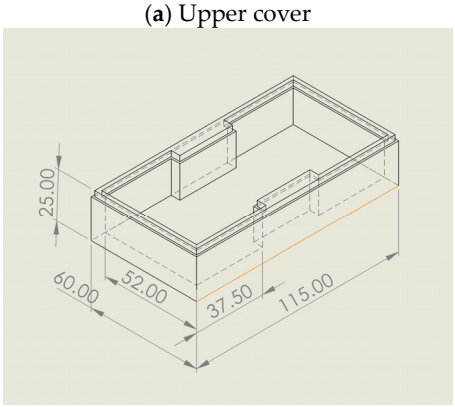
Figure 16. Fourth-generation design of an anti-explosion shell for electronic connectors.

In order to allow for airtight assembly and easy usage of the anti-explosion shell, a tenon design was adopted. Because of the excellent spatial resolution of FDM 3D printers, the thickness of the tenon wall was only a thousandth of a meter, which allowed us to effectively reduce the weight of the aerovehicle. Incorporating all these considerations, the type of device evolved over several different generations of designs. The special design of the tenon in the fourth-generation design for an anti-explosion shell is shown in Figure 16b,c. The thickness and height of the tenon were modified to enhance the installation strength and ensure airtightness based on the deficiencies of the previous designs (red frame in Figure 16b). Thus, a thicker tenon was designed to meet the strength requirement.

The fourth-generation design for the anti-explosion shell of a flight control board is shown in Figure 17a,b. This design mainly increases the front space to allow it to store whole wires. It also increases the height and thickness of the shell to enhance the airtightness. The modified position of the thicker tenon is shown in the red frame in Figure 16a.



(**a**) Upper cover



(**b**) Lower cover

Figure 17. Fourth-generation design of an anti-explosion shell for the flight control board.

3.3.2. Manufacturing Process

The first-generation anti-explosion device developed in this study is shown in Figure 18. The two primary design parameters were the shell volume and reducing the weight. The measurements of joints with different sizes were used in creating the design. The main principle of anti-explosion designs is to avoid direct contact between flammable gases and electrical junctions, i.e., the fire source and fuel, which are two of the three elements of combustion.

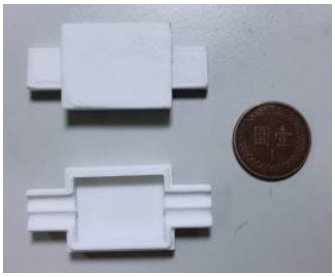
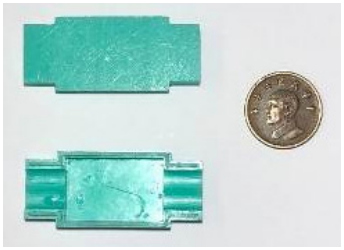


Figure 18. First-generation design of the anti-explosion shell.

The preliminary design needed to be easy to disassemble and assemble to allow for easy replacement of the device. Therefore, upper and lower covers were used. The airtightness between these covers was used as a metric to assess the safety of the anti-explosion device design. However, the margin of the first-generation design was not sufficient, and the printing limitations and potential errors of 3D printer hardware were not considered. This caused the connector not to connect to the electrical wires as expected. The second-generation anti-explosion shell design is shown in Figure 19.



(**a**) Electrical wire connector



(**b**) Flight control board

Figure 19. Second-generation design of anti-explosion shell (shown with Taiwanese one-dollar coin for comparison).

The electrical anti-explosion concepts used in the first-generation design were included in the second-generation shell design, which addressed the insufficient size margin. The internal volume of the shell was increased within the allowable range to provide more space for the installation of the connector and wire. However, the preliminary test revealed that the thickness of the shell wall and the density of the material were not enough to sustain operation and quick disassembly. This will cause rupture of the boundary after usage, and a sufficient airtightness will not be achieved. Based on the previous test results, the third-generation shell design addressed the disadvantages of the first- and second-generation designs. The internal space and thickness were increased within the allowable range to improve the space margin and thickness. In addition, the anti-explosion shell should effectively prevent contact between sparks on the UAV and flammable gases in the environment while minimizing the additional weight on the UAV through achieving the appropriate size and fit. This will enable the UAV to perform its tasks more flexibly. The anti-explosion shell designs for electrical wire connections and flight control boards are shown in Figures 20 and 21, respectively. The final installation of the anti-explosion devices on a UAV is shown in Figure 22. The total weight of the devices was less than 300 g. In contrast, the weight of a typical industrial anti-explosion device is too heavy to use on UAVs. For UAVs with a strict weight limit, the developed device can satisfy both the weight and anti-explosion requirements. Therefore, it could be a valuable component for industrial-grade vehicles.

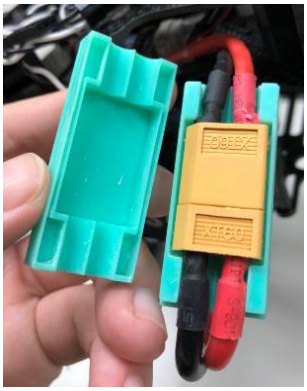


Figure 20. Anti-explosion device for electrical wire connectors.

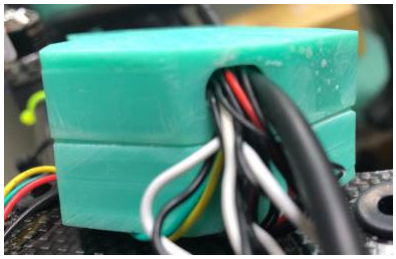


Figure 21. Anti-explosion device for the flight control board.



Figure 22. Complete installation of anti-explosion devices on a UAV.

3.3.3. Applicability of the Designed Device and Regulations

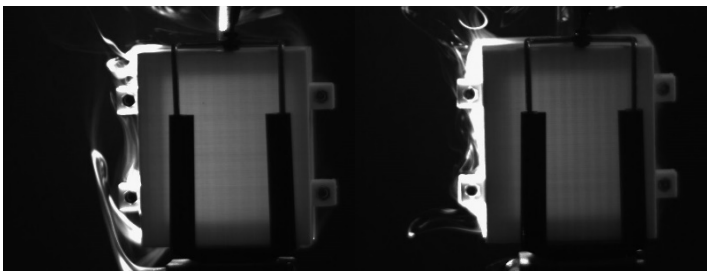
Based on the regulations outlined in Appendix A, the applicability of the design devices and their adherence to regulations will be discussed in detail in this section. Initially, the intrinsically safe anti-explosion code i was thought to be more suitable for assessing the developed devices, especially the electrical circuit or low-power electrical appliance requirements. Except for the electrical motor, the control line on UAVs typically consumes a small amount of energy, usually less than 450 W, and the voltage is less than 50 volts. Theoretically, this voltage is a safe voltage as it is harmless and hard to pose a hazard. Consequently, the operating conditions of the UAV can meet the regulations for being intrinsically safe from explosions.

The MESG requirements were assessed through measurements of porosity and leakage. For carbon fiber, the MESG between fiber layers was about 3.39 to 3.42 Å (1 Å = 10^{-10} m). This size is much smaller than the particle size of ethylene gas. As for PLA, its porosity is typically small because it is a plastic. Ethylene gas cannot pass through the pores of plastic. Therefore, leakage is only possible at the gap between the upper and lower covers and needs to be prevented in the designed devices. In addition, the filling degree of the 3D printer was set to a larger layer infill to decrease the stacking distance and prevent gas particles from passing through this space. In general, the filling degree of common products is about 20%. In this study, the percentage was set to 60–80% to enhance the structural density; dust and gas particles cannot penetrate the surface of this material.

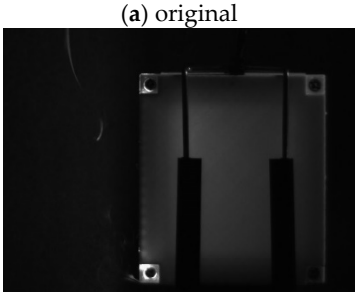
In order to conform to regulations, the spatial resolution of the FDM 3D printer was set to $\pm$0.05 mm, which can help in printing tenons with a thin boundary. The design of the tenon was the primary mechanism to prevent gas leakage. Combined with rubber and a proper flame retardant, the device could prevent leakage along the side of the tenon between the upper and lower covers. However, it is difficult to experimentally determine whether gas particles can infiltrate into the anti-explosion device. The high-pressure

visualization method proposed by Yeh et al. [22] was used to visualize the flow properties at different positions. Using the appropriate gas pressure, smoke is brought to specific positions to visualize any leakage. The input high-pressure smoke follows the original fluid flow smoothly without jerky perturbations. Therefore, this method was used to introduce high-pressure smoke into the anti-explosion device to check for smoke leakage. The main lighting system consists of a combination of a 1 W semiconductor laser and a cylindrical lens. A high-speed CMOS camera was used to capture time sequence pictures. The particle size of the heated atomized oil droplet smoke was measured to be about 2.5~6 nm, which is similar to that of ethylene gas (a group II gas). Thus, the oil droplet smoke can be used to replace ethylene gas and was used as the fluid for the visualization experiment.

The results of the gas leakage experiment under different conditions are shown in Figure 23a,c. The input pressure after fine-tuning was set to about 3 atm, which is similar to the explosion pressure of ethylene gas. As shown in Figure 23a,b, the smoke leaked from the border and corner because of insufficient airtightness. After checking the tightness of the border and corner, the rubber and tenon were found to be insufficiently merged. The smoke leaked through this small gap under high-pressure conditions. As shown in Figure 23c, there was no leaking smoke at the device boundary after tightness enhancement. These experimental results verify that the designed devices satisfy the MESG requirements. The final design of the anti-explosion device is shown in Figure 24.



(**a**) original (**b**) with tenon



(**c**) with rubber and tenon

Figure 23. Smoke leakage experiments under 3 atm input pressure.

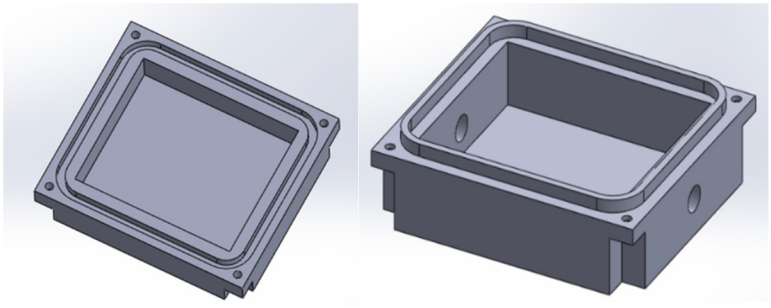


Figure 24. Final design of anti-explosion devices.

Besides gas leak prevention, the anti-explosion devices should also prevent internal explosions. For a thin and small volume device, the pressure caused by the explosion

could be assumed to be one-dimensional pressure transmission. Under the assumption of uniform pressure distribution, the pressure caused by an explosion could be evenly distributed on the surface. These intensity values are much lower than the tensile strength of the two used materials [23]. Consequently, it can be confirmed that the tensile intensity of the materials used in this study is enough to address the tension caused by gas expansion during explosion, such as the explosion pressure level definition of propane and ethylene shown in NFPA 68. In addition, the internal volume of the anti-explosion device is small, making the potential gas leak volume percentage too small to induce an explosion inside the device. Even if an explosion happens, the material can still absorb the explosion energy, and its airtightness can also prevent the arc spark from passing through the gap of the device and becoming a fire source. Based on this, the developed anti-explosion devices satisfy the relevant regulations preliminarily.

4. Conclusions

Three-dimensional printing is the most commonly used method for manufacturing customized or mock-up products for industrial applications. In particular, aviation devices for drones usually require a high spatial resolution to satisfy the small size requirement. In order to improve the printing quality, a simulative wind tunnel was constructed to investigate the effects of atmosphere control inside the chamber during the printing process. Acrylic was used as the main material of the wind tunnel, and all the connection parts were made using PLA via FDM 3D printing. A constant-temperature hot-wire anemometer was used to measure velocity. In the experiments, a tapered deflector was installed inside the expansion section to more evenly distribute the internal airflow. After this modification, the velocity distributions at the nozzle outlet were considerably improved. However, the experimental results using dual-output nozzles also revealed that the velocities at the upper and lower output nozzles were not consistent. However, interestingly, the velocity measurements agreed with the requirements. Dual-output nozzles with different tilde angles were used to simultaneously affect the proximal and distal positions in the printing area. It was found that higher output velocities from the upper nozzle allow for atmosphere control and maintenance of airflow at the distal position. Meanwhile, a lower velocity could satisfy the requirements for the proximal position. The experimental results also showed that the temperature variation was smooth and that the effect of temperature is slightly dependent on the distance from the nozzle. The quality of the FDM 3D-printed product can be maintained using this control method. To achieve a better performance of this atmosphere control method, a compound nozzle with different tilde angles was installed; the nozzle with an upper nozzle with a 30-degree angle and a lower nozzle with a 45-degree angle showed the best performance. It could simultaneously affect the proximal and distal positions, with a strong cooling effect even at a distance from the nozzle.

Anti-explosion devices for multi-rotor UAVs were produced using the developed method to fulfill the accuracy requirements. The electrical contacts on the UAV that can easily produce arcing should be protected to reduce the hazard risk when the UAV is operating in industrial environments. The weight limitation of the UAV was also considered. All the designs were modeled on a computer to allow for modification of key design parameters. Due to the resolution requirement, the FDM 3D printer was customized with a limited spatial resolution of ± 0.05 mm, which can also satisfy the basic MESG requirement. The FDM printer was also equipped with atmosphere control technology to enhance the printing quality by maintaining a constant temperature. In addition, the developed devices fully meet the anti-explosion regulations based on the porosity analysis, smoke leakage experiment, and material tensile test. The prototype design should facilitate disassembly and assembly in case the device needs to be replaced. Therefore, a design with upper

and lower covers was adopted. Sufficient airtightness between the covers is necessary for the device to prevent explosions. Four generations of designs for the anti-explosion shell were generated, with each successive generation addressing the disadvantages of the previous generations. The internal space and thickness were drastically enlarged within the allowable range to improve the space margin and thickness. The structural design of the tenon ensured the airtightness of the upper and lower covers.

The experimental results reveal that atmosphere control can efficiently enhance the print quality and that the print resolution of a commercial FDM 3D printer can be improved effectively. In the anti-pressure testing via a high-pressure smoke experiment, the manufactured anti-explosion devices for drones demonstrated a sufficient intrinsic safety level, suggesting that they can be used in UAVs performing daily inspections of pipelines in petrochemical plants. The two main contributions of this study are the development of a practical method for improving FDM 3D printers and anti-explosion devices for drones.

5. Future Work

Based on the results of this study, there are several future research directions to pursue to achieve the application of anti-explosion technology for multi-rotor UAVs.

- Studies can test whether a carbon composite material can be used to replace PLA to further reduce the weight and usage intensity.
- The smoke flow visualization method can be used to visualize smoke leakage at the shell boundary to test methods to improve the airtightness.
- In addition to actual flight tests in a factory, third-party standardization certification work should be carried out. This certification could promote wider industrial application of the anti-explosion shell and improve inspection methods in the petrochemical field.
- A suitable fireproof filling material to prevent gas leakage should be identified.
- The weight of the device should be further reduced while maintaining its strength.

Author Contributions: Methodology, H.-P.C.; Investigation, H.-P.C. and Y.-L.Y.; Resources, H.-P.C.; Writing—review & editing, Y.-L.Y.; Visualization, Y.-L.Y.; Project administration, Y.-L.Y. All authors have read and agreed to the published version of the manuscript.

Funding: This research received no external funding.

Data Availability Statement: The original contributions presented in this study are included in the article. Further inquiries can be directed to the corresponding author.

Conflicts of Interest: The authors declare no conflicts of interest.

Appendix A

Appendix A.1. Division of Safety Zones

The safety of industrial environments in terms of explosions is mainly categorized into explosive and hazardous regions.

1. Explosive atmosphere: There is a mixture of flammable substances in the air in the form of gas, vapor, dust, fibers, or flying floc under normal atmospheric conditions. An explosion will propagate continuously after being ignited.
2. Hazardous area: An area with an explosive environment or an environment where the construction and installation of electrical equipment need special precautions.

The descriptions and time definitions of each zone are given in Table A1. For UAVs, anti-explosion devices should be designed for operation in zones 1 and 2, i.e., they should prevent spark leakage from electrical connectors in environments rich in flammable gases.

Table A1. Description and time definition of different zones [24].

Zone	Description	Time Definition (Hr/Year)
0 (gas) 20 (dust)	Explosive environment exists constantly, for a long time, or often	>1000
1 (gas) 21 (dust)	An explosive environment may exist under normal operation	10~1000
2 (gas) 22 (dust)	An explosive environment is unlikely to exist or only exists for a very short period of time under normal operation	0.1~10

Appendix A.2. Considerations for Anti-Explosion Devices

In Taiwan, the national identification label for industrial anti-explosion electrical devices is mainly based on the IEC specifications. It includes not only all anti-explosion codes, types, equipment attribution, and operation temperature classification, but also the Industry Bureau Exclusive Mark. The national standard label of anti-explosion devices for Taiwan is shown in Figure A1. All verified devices should be labeled with this mark to show their specifications and application area. However, there are no marks in any country for anti-explosion devices for UAVs.

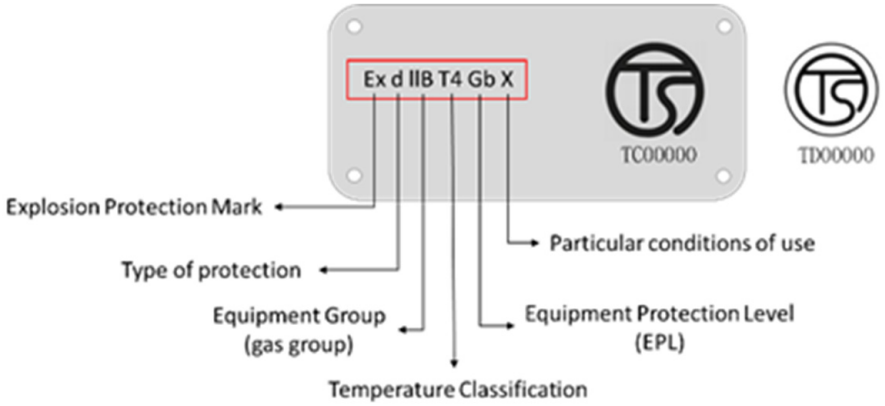


Figure A1. Industrial Bureau anti-explosion type verification and specification mark [24].

Based on the types of protection listed in Table A2, the intrinsically safe type (code i) aligns with the devices designed in this study. Similar to anti-explosion devices for electrical circuits or low-power electrical appliances, the device should prevent UAVs from becoming a fire source and inducing an explosion of surrounding gas under normal or abnormal operation. UAVs are mainly seen as low-power devices except for some of their non-essential equipment. Their operating voltage is typically lower than 40 volts.

Table A2. Application area for each type of protection [24].

Type of Protection	Definition	Application Area
Intrinsic Safety "1"	1. It is designed for electronic circuits or low-energy electrical appliances. It will not cause dangerous gas to explosion around the instrument and circuit under normal and non-normal conditions. 2. The energy of output and input of the intrinsically anti-explosion electronic circuit are all designed to be below the energy that is not enough to ignite hydrogen to explosion.	Zone 0 (ia) Zone 1 (ia, ib) Zone 2 (ia, ib)
Oil Immersion "o"	1. The voltage transformer is installed in the shell and insulated with high ignition point insulating oil to achieve anti-explosion consequent. 2. This kind of equipment with poor reliability is rare to be used at present.	Zone 1 Zone 2
Powder Filling "q"	1. The devices such as capacitors, resistors, small transformers installing in the shell are filled with fine sand to isolate and achieve anti-explosion consequent. 2. The structure can not be used individually, and it is all used inside the Exe shell.	Zone 1 Zone 2
Encapsulation "m"	1. The polyester will be injected inside the components which will generate sparks or overheat temperature rising devices, and the surface of overall shell will never produce sparks or overheat temperature rising which will cause explosion due to dangerous gas.	Zone 1 Zone 2

The classification of the induced flame propagation limit of explosive gases is based on the IEC standard and the following (Table A2):

[1] Clearance size: the flame in the explosive mixed gas will transmit to the other side through the gap.
[2] Pressure and temperature of the gas and its composition.

This classification is important for the design of anti-explosion devices for electrical circuits.

As shown in Table A3, the maximum experimental safety gaps (MESGs) for different kinds of explosive gases differ. A schematic diagram of the maximum experimental safety gap is shown in Figure A2. Representative gases are listed in Table A4. A comparison of the temperature grade in the specification label is shown in Table A5, which indicates that the safety margin for the maximum surface temperature for the T1 and T2 groups in group II is below 10 K, and for the T3 to T6 groups, it is lower than 5 K. The gap of an anti-explosion device is the main point to be considered in its design for spark leakage prevention; it was also verified in this study.

Table A3. Maximum safety gap of different explosive gases [24].

Explosive Gas Group	Maximum Experimental Safety Gap (mm)
II A	≥0.9
II B	0.5~0.9
II C	≤0.5

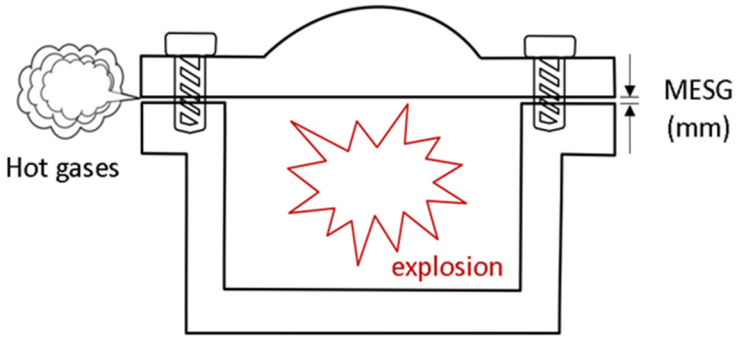


Figure A2. Schematic diagram of MESG.

Table A4. Representative explosive gases of different groups [24].

Group	Representative Element
I	Methane
II A	Propane
II B	Ethylene
II C	Hydrogen

Table A5. Temperature grades [24].

Temperature Class	Max. Surface Temperature
T1	≤450 °C
T2	≤300 °C
T3	≤200 °C
T4	≤135 °C
T5	≤100 °C
T6	≤85 °C

Explosive environments can contain explosive gas, explosive powder, or biogas. The protection standard for equipment is CNS-3376-14; the protection level codes for different devices are shown in Table A6. For UAVs flying in petrochemical environments, the UAV body should be designed to prevent the UAV from being an ignition source. Thus, the "high" and "very high" protection levels are not sufficient; "enhanced" is the appropriate level.

Table A6. Protection level code for devices [23].

Equipment Protection Level	Standard
Ma	The equipment installed in the mine pit that is susceptible to biogas, having a 'very high' level of protection and sufficient safety protection. During the normal operation or expected failure, or during the failure period, even when the gas blasts and no energise, It can not be a source of ignition.
Mb	The equipment installed in the mine pit that is susceptible to biogas, having a 'high' level of protection and sufficient safety protection. During the normal operation or expected failure or during the failure period, even when the gas blasts and no energise, it can not be a source of ignition.

Table A6. *Cont.*

Equipment Protection Level	Standard
Ga	Equipment for explosive gas atmospheres, having a 'very high' level of protection, which is not a source of ignition in normal operation, expected faults, or when subject to rare faults.
Gb	Equipment for explosive gas atmospheres, having a 'high' level of protection, which is not a source of ignition in normal operation, or when subject to faults that may be expected, though not necessarily on a regular basis.
Gc	Equipment for explosive gas atmospheres, having an 'enhanced' level of protection, which is not a source of ignition in normal operation and which may have some additional protection to ensure that it remains inactive as an ignition source in the case of regular expected occurrences, for example, failure of a lamp.
Da	Equipment for explosive dust atmospheres, having a 'very high' level of protection, which is not a source of ignition in normal operation, expected faults, or when subject to rare faults.
Db	Equipment for explosive dust atmospheres, having a 'high' level of protection, which is not a source of ignition in normal operation, or when subject to faults that may be expected, though not necessarily on a regular basis.
Dc	Equipment for explosive dust atmospheres, having an 'enhanced' level of protection, which is not a source of ignition in normal operation and which may have some additional protection to ensure that it remains inactive as an ignition source in the case of regular expected occurrences, for example, failure of a lamp.

Table A7. Applicable groups and areas for different equipment protection levels [23].

Equipment Protection Level	Group	Applicable Hazardous Area
Ma	I	Mining Industry
Mb		
Ga, Da	II, III	Zones 0, 20
Gb, Db		Zones 1, 21
Gc, Dc		Zones 2, 22

References

1. Shahrubudin, N.; Lee, T.C.; Ramlan, R.J.P.M. An Overview on 3D Printing Technology: Technological, Materials, and Applications. *J. Procedia Manuf.* **2019**, *35*, 1286–1296. [CrossRef]
2. Ngo, T.D.; Kashani, A.; Imbalzano, G.; Nguyen, K.T.; Hui, D. Additive manufacturing (3D printing): A review of materials, methods, applications and challenges. *J. Compos. Part B Eng.* **2018**, *143*, 172–196. [CrossRef]
3. The History of 3D Printer: From Rapid Prototyping to Additive Fabrication. Available online: https://www.sculpteo.com/blog/2017/03/01/whos-behind-the-three-main-3d-printing-technologies/ (accessed on 20 February 2021).
4. Tarancón, A.; Esposito, V.; Torrell, M.; Di Vece, M.; Son, J.S.; Norby, P.; Bag, S.; Grant, P.S.; Vogelpoth, A.; Linnenbrink, S.; et al. 2022 roadmap on 3D printing for energy. *J. Phys.* **2022**, *4*, 11501. [CrossRef]
5. Kuntjoro, W.; Roslan, I.S.; Muta'ali, A.B.A.; Anwar, N.A.K.; Nasir, R.E.M. A Study of 3D Printed Box Structure. *J. Aeronaut. Astronaut. Aviat.* **2021**, *53*, 137–142. [CrossRef]
6. Kuntjoro, W.; Latip, U.H.; Nasir, R.E.; Ramly, R. Static Analysis of 3D-Printed Sub Wing Box Lug Joint Assembly using Finite Element Method. *J. Aeronaut. Astronaut. Aviat.* **2022**, *54*, 335–346. [CrossRef]
7. Kabbe, N.; Lohar, A.; Panchaxarimath, A.; Tiwary, V. Revolutionizing Aerospace Industries through Additive Manufacturing: Innovations, Challenges, and Prospects. *J. Aeronaut. Astronaut. Aviat.* **2024**, *56*, 593–602. [CrossRef]

8. Wang, W.C.; Chang, C.Y. Flow analysis of the laminated manufacturing system with laser sintering of metal powder. Part I: Flow uniformity inside the working chamber. *J. Adv. Manuf. Technol.* **2017**, *92*, 1299–1314. [CrossRef]
9. Lee, C.Y.; Liu, C.Y. The influence of forced-air cooling on a 3D printed PLA part manufactured by fused filament fabrication. *J. Addit. Manuf.* **2019**, *25*, 196–203. [CrossRef]
10. Joshi, S.C.; Sheikh, A.A. 3D printing in aerospace and its long-term sustainability. *J. Virtual Phys. Prototyp.* **2015**, *10*, 175–185. [CrossRef]
11. Tay, Y.W.D.; Panda, B.; Paul, S.C.; Noor Mohamed, N.A.; Tan, M.J.; Leong, K.F. 3D printing trends in building and construction industry: A review. *J. Virtual Phys. Prototyp.* **2017**, *12*, 261–276. [CrossRef]
12. Yampolskiy, M.; Skjellum, A.; Kretzschmar, M.; Overfelt, R.A.; Sloan, K.R.; Yasinsac, A. Using 3D printers as weapons. *Int. J. Crit. Infrastruct. Prot.* **2016**, *14*, 58–71. [CrossRef]
13. Smith, J.W.; Johnson, D.R.; Müller-Vonmoos, M. Dolomite for determining atmosphere control in thermal analysis. *J. Thermochimica Acta* **1974**, *8*, 45–56. [CrossRef]
14. Spriggs, G.E. The Importance of Atomophere Contol in Hard-Metal Production. *Powder Metall.* **1970**, *13*, 369–393. [CrossRef]
15. Kingon, A.I.; Clark, J.B. Sintering of PZT Ceramics: I, Atmosphere Control. *J. Am. Ceram. Soc.* **1983**, *66*, 253–256. [CrossRef]
16. Kanazawa, S.; Eto, K.; Imagawa, W.; Akamine, S.; Ichiki, R. 3D-Printed Atmospheric-Pressure Plasma Reactors. In Proceedings of the 3rd Korea-Japan Conference on Plasma and Electrostatics Technologies, Jeju, Republic of Korea, 7 November 2014.
17. Jerez-Mesa, R.; Gomez-Gras, G.; Travieso-Rodriguez, J.A.; Garcia-Plana, V. A comparative study of the thermal behavior of three different 3D printer liquefiers. *J. Mechatron.* **2018**, *56*, 297–305. [CrossRef]
18. Salehi, M.; Maleksaeedi, S.; Nai, M.L.S.; Gupta, M. Towards additive manufacturing of magnesium alloys through integration of binderless 3D printing and rapid microwave sintering. *J. Addit. Manuf.* **2019**, *29*, 100790. [CrossRef]
19. Kalms, M.; Narita, R.; Thomy, C.; Vollertsen, F.; Bergmann, R.B. New approach to evaluate 3D laser printed parts in powder bed fusion-based additive manufacturing in-line within closed space. *J. Addit. Manuf.* **2019**, *29*, 161–165. [CrossRef]
20. Dong, J.; Li, Y.; Lin, P.; Leeflang, M.A.; Van Asperen, S.; Yu, K.; Tümer, N.; Norder, B.; Zadpoor, A.A.; Zhou, J. Solvent-cast 3D printing of magnesium scaffolds. *J. Acta Biomater.* **2020**, *114*, 497–514. [CrossRef]
21. Li, H.; Liu, Y.; Liu, Y.; Zeng, Q.; Hu, K.; Lu, Z.; Liang, J. Effect of debinding temperature under an argon atmosphere on the microstructure and properties of 3D-printed alumina ceramics. *J. Mater. Charact.* **2020**, *168*, 110548. [CrossRef]
22. Yeh, Y.L. Development of the High-pressure Smoke Visualization and Its Verification at Low Reynolds Number. *J. Aeronaut. Astronaut. Aviat.* **2014**, *46*, 61–66. [CrossRef]
23. Yeh, Y.L. On the Standard Strength Test of 3D Printing Materials Applied for UAV Propellers. *Mod. Phys. Lett. B* **2020**, *34*, 2040017. [CrossRef]
24. Available online: https://www.sancs.com/services_certified_2.php (accessed on 16 January 2020).

Disclaimer/Publisher's Note: The statements, opinions and data contained in all publications are solely those of the individual author(s) and contributor(s) and not of MDPI and/or the editor(s). MDPI and/or the editor(s) disclaim responsibility for any injury to people or property resulting from any ideas, methods, instructions or products referred to in the content.